RESEARCH ARTICLE | OCTOBER 16 2023

In situ TEM heating experiments on thin epitaxial GeSn layers: Modes of phase separation

Karí Martínez ; Alexey Minenkov ; Johannes Aberl ; Dan Buca ; Moritz Brehm ; Heiko Groiss

APL Mater. 11, 101117 (2023)
https://doi.org/10.1063/5.0167407

In situ TEM heating experiments on thin epitaxial GeSn layers: Modes of phase separation

Cite as: APL Mater. 11, 101117 (2023); doi: 10.1063/5.0167407
Submitted: 12 July 2023 • Accepted: 28 September 2023 •
Published Online: 16 October 2023

Karí Martínez,[1,a] Alexey Minenkov,[1,a] Johannes Aberl,[2] Dan Buca,[3] Moritz Brehm,[2] and Heiko Groiss[1]

AFFILIATIONS

[1] Christian Doppler Laboratory for Nanoscale Phase Transformations, Center for Surface and Nanoanalytics, Johannes Kepler University Linz, Altenberger Straße 69, 4040 Linz, Austria
[2] Institute of Semiconductor and Solid-State Physics, Johannes Kepler University Linz, Altenberger Straße 69, 4040 Linz, Austria
[3] Peter Grünberg Institute (PGI-9) and JARA-Fundamentals of Future Information Technologies, Forschungszentrum Jülich, 52428 Jülich, Germany

[a] **Authors to whom correspondence should be addressed:** kari.martinez_reyna@jku.at and oleksii.minienkov@jku.at

ABSTRACT

The thermal stability of GeSn epitaxial thin films was investigated via *in situ* transmission electron microscopy (TEM). Samples were grown with a similar layer structure and 10 at.% Sn content by either molecular beam epitaxy or chemical vapor deposition. Despite the same layer thickness and concentration, the decomposition mode differs dramatically for each GeSn sample during annealing experiments. We observed that the sample with a Ge buffer on a Ge substrate is structurally stable up to 500 °C, while above this temperature, β-Sn precipitates appear, indicating a decomposition mechanism of solid-state precipitation. On the other hand, the second sample exhibited high susceptibility to Ga ion incorporation during the focused ion beam TEM specimen preparation, which is attributed to a high defect density owing to an atypically thin Ge buffer layer grown on a Si substrate. In this case, the efficient phase separation in the sample was facilitated by Ga contamination, promoting the appearance of a GaSn-based liquid phase at a temperature as low as 200 °C. The decomposition temperatures found and the occurrence of the two different decomposition modes are discussed in relation to the experimental methods used.

I. INTRODUCTION

The interest in GeSn alloy epilayers is based on their great potential in high-performance Si-based electronics and optoelectronics. Germanium, being compatible with the standard Si-CMOS technology, has an indirect bandgap, which can be tuned to a direct bandgap by alloying Ge with Sn.[1–3] According to recent results,[4] the transition to a direct bandgap semiconductor is observed by incorporating Sn content above 6 at.%. However, the desired alloys are unstable at high temperatures, posing severe limitations to their synthesis and application.[5] Knowing the thermal budget to which a $Ge_{1-x}Sn_x$ sample can be exposed before triggering Sn segregation is of principal importance, considering that the material will be subjected to additional heating during device fabrication[6,7] and operation. One powerful tool, which allows for studying the effects of thermal annealing and observing related dynamic processes in materials, is *in situ* transmission electron microscopy (TEM). This technique uses electron transparent specimens placed on micro-electronic mechanical system (MEMS) chips that allow for applying various stimuli. The focused ion beam (FIB) lift-out technique is suitable for transferring specimens to MEMS chips.[8] However, Ga^+ FIB milling can also produce artifacts in the sample through the interaction of the ions,[9] such as amorphization and Ga implantation.[10]

In this Letter, using *in situ* TEM heating, we investigate the stability of GeSn epilayers of different structural qualities but with similar thickness and Sn concentration. The two main methods for growing GeSn thin epitaxial layers with high Sn content are molecular beam epitaxy (MBE) and chemical vapor deposition (CVD). Each method has its advantages: by MBE, thin films of GeSn alloys with higher Sn concentration can be grown,[11] while CVD films exhibit superior optical properties,[12–14] making them preferable for

application in real-world devices. For instance, all GeSn-based lasers to date were grown, to our best knowledge, via CVD.[15,16] The reasons behind the very different properties of the material grown by these two methods are still under debate. Generally, both use low growth temperatures to suppress Sn segregation, which can introduce point defects,[17] which, together with dislocations,[18] can affect the properties of the layers. In the case of CVD specimens, to use readily available Si substrates, relatively thick Ge buffers of about 2.5 μm can create the so-called virtual substrates, which minimizes the density of threading dislocations of about 10^7 cm^{-2}.[19] This is believed to be advantageous for its optical properties.[13] In Ref. 13, the properties of GeSn samples grown by MBE and CVD were investigated, with the limitation that the substrates and the layer structure of the samples are different, which makes it difficult to compare their performance unambiguously. Even though more threading dislocations were found in CVD samples than in MBE, the optical properties of the CVD specimens were still better. One reason for the inferior performance of MBE-grown GeSn samples could be attributed to the presence of point defects. These will always be present in MBE-grown samples grown at ultra-low growth temperatures and could only be successfully suppressed by growth pressures deep in the ultra-high-vacuum range.[20,21]

In this work, we study the thermal stability of two GeSn samples with an intended similar structure, grown by MBE and CVD. The quality and performance of the CVD-grown sample are not representative of the state-of-the-art GeSn thin layer growth due to the atypical Ge thin buffer layer used. However, the layers allow us to investigate the impact of defects on the achieved thermal stability of GeSn epilayers and to generally discuss the occurring decomposition modes depending on the experimental geometry, which includes pointing at the challenges of conventional Ga^+ FIB specimen preparation for *in situ* TEM experiments.

II. METHODS

The Sn content and thickness of the Ge buffer and GeSn layer of the investigated samples were selected to be ≈10 at.%, ≈200 nm and ≈50 nm, to reduce the number of variables in the heating experiments. Sample A was grown by MBE in a Riber SIVA-45 solid-source MBE (Riber, France), i.e., equipped with an electron beam evaporator for Ge deposition and a Sn effusion cell. The preparation of the commercial UmicoreCz-Ge (001) substrate (cut into 9 × 9 mm^2 pieces) started with a solvent-based cleaning process. Once loaded into the MBE chamber, Ge substrates were degassed for 30 min at 300 °C and then heated for 15 min at 750 °C for thermal oxide desorption. Then, the substrate temperature was lowered to 320 °C to deposit a 200 nm thick Ge buffer layer at a growth rate of 0.15 Å/s. The growth temperature used for the nominally 50 nm thick GeSn layer was 150 °C, keeping a Ge deposition rate of 0.15 Å/s, while the Sn source was operated at a temperature of 1073 °C. Sample B was grown by CVD on a 200 mm Si wafer (100) using reactive gas source epitaxy in an industry-compatible reactor with a showerhead gas delivery design, which assured a homogeneous precursor distribution on top of the full wafer. Before growth, the native oxide was removed *ex situ* in a fully automated single-wafer cleaning tool based on HF (hydrofluoric acid) vapor chemistry. Additionally, an *in situ* hydrogen bake was performed at 1000 °C, ensuring a contaminant-free wafer surface fit for epitaxy. To prevent issues related to the large lattice mismatch between GeSn and Si, the films were grown on top of a Ge buffer layer deposited at 450 °C. However, this buffer layer was only 180 nm thick, for which a resulting high defect density can be expected. This allows us to study defects' influence on the decomposition behavior in TEM *in situ* experiments. The precursor gases used for the GeSn layer growth were digermane (Ge_2H_6) and tin tetrachloride ($SnCl_4$), which ensured high growth rates of about 1.67 Å/s at temperatures as low as 340 °C, necessary for the suppression of Sn segregation.

A ZEISS Crossbeam 1540XB (ZEISS, Germany) scanning electron microscope (SEM) with FIB add-on was used to prepare the TEM lamellae on the MEMS chip (Wildfire nano-chip from DENSsolution, Netherlands). For conventional FIB lamella preparation, pieces of 1.5 × 1.5 mm^2 were sliced; then, the surface of GeSn was covered with an amorphous carbon layer followed by a 30 nm thick W layer, which was deposited with magnetron sputtering via Compact Coating unit CCU-010 HV (Safematic, Switzerland). The W precursor, which is more stable in heating experiments as compared to Pt, was used throughout a FIB lift-out procedure. The MEMS chip was prepared following the steps described in Ref. 8.

The *in situ* TEM heating experiments were carried out in a JEOL JEM-2200FS (JEOL, Japan) operated at an acceleration voltage of 200 kV. The TEM is equipped with an in-column Ω-filter and a TemCam-XF416 (TVIPS, Germany) CMOS-based camera. Elemental maps were constructed in the scanning (S)TEM mode via an X-MaxN 80T energy dispersive x-ray spectroscopy (EDXS) detector from Oxford Instruments using Aztec software. The *in situ* heating experiments were performed within a wide temperature range of 25–600 °C with a ramp of 5 °C/s. After each heating step, the samples were cooled to 25 °C. For the considered steps, the respective temperature has been maintained for 30–60 min each, the time necessary to acquire EDXS maps and to conduct high-resolution (HR)TEM investigation. According to the MEMS-based chips manufacturer specification, the measurement error did not exceed 5%.[22]

III. RESULTS AND DISCUSSION

The evolution of the two samples was investigated in a cross-sectional geometry via *in situ* TEM heating. First, both samples prepared by the conventional FIB technique and transferred to MEMS chips were characterized by STEM EDXS at room temperature. The EDXS maps are shown in Fig. 1, representing a well-defined layer structure: the W capping layer deposited by FIB, the GeSn layer, the Ge buffer, and the substrate. Sample A has a measured thickness of 48 nm and contains 10 at.% Sn. In addition, it was possible to confirm that this sample is strained and that no dislocations are present. For sample B, the GeSn layer is 40 nm thick with a Sn content of 11.5 at.%, and it was possible to identify threading dislocations in the Ge buffer and the GeSn layer.

Unavoidably, Ga is present in both samples due to preparation by FIB.[23,24] The elemental maps (Fig. 1) show that Ga in sample A is presented only in the W capping layer. For sample B, though, Ga was additionally detected in all epitaxially grown layers. For instance, the

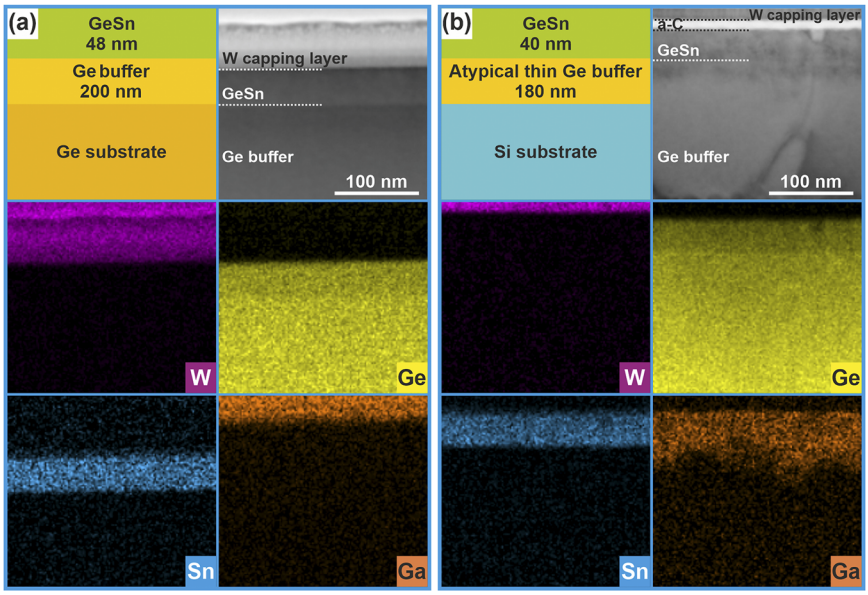

FIG. 1. The layer structure, STEM images, and corresponding EDXS element maps of the cross sections of (a) sample A and (b) sample B. W corresponds to the capping layer, and Ga corresponds to the ion contamination due to the FIB preparation.

Ga concentration detected in the GeSn layer area of sample B is ~6.5 at.%, compared to a Ga concentration of less than 1.5 at.% presented in the GeSn layer of sample A. Using the same sample preparation protocols, the different incorporation of Ga into the crystal structure by, e.g., implantation or diffusion during the specimen preparation strongly suggests different defect types or defect densities in the two samples.

By HRTEM and applying fast Fourier transform (FFT) analysis, we first traced the structural changes in sample A depending on the temperature. The FFT at room temperature [Fig. 2(a)] shows the structure orientated along the [110] zone axis, which remains unchanged at temperatures below 500 °C. At above 500 °C, Sn segregation induces precipitation of an additional phase. This event can be observed in the HRTEM images [Fig. 2(b)] taken after cooling

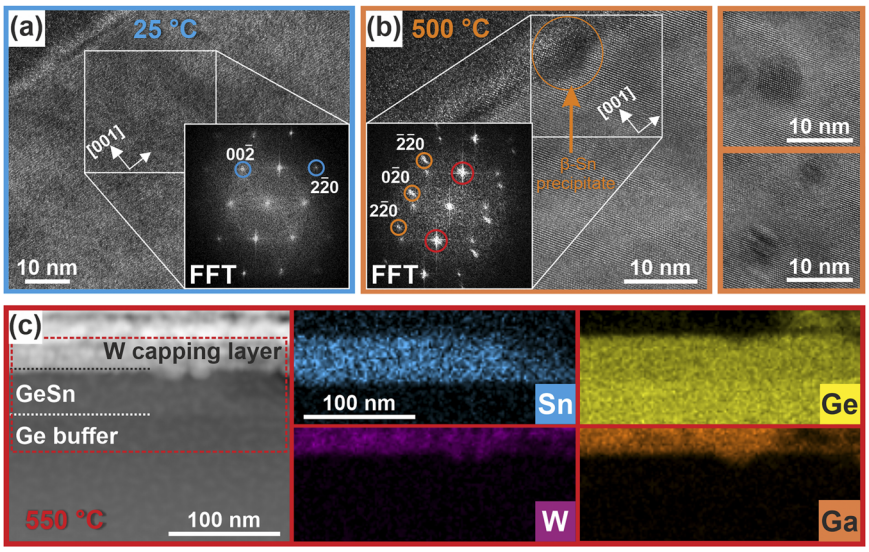

FIG. 2. HRTEM and FFT of sample A: (a) At room temperature, where FFT shows a characteristic diffraction pattern of the zone axis [110]. The specimen is stable below 500 °C. (b) Images taken at room temperature after annealing at 500 °C; reflexes of β-Sn (200) and (220) planes (highlighted with orange circles) can be found in FFT. (c) HAADF STEM and EDXS maps reveal the diffusion of Ge toward the W capping layer at 550 °C.

the sample to room temperature and by the appearance of new reflexes, highlighted with orange circles in the FFT of this area. These reflexes are well-fitted with the β-Sn crystal structure oriented along the [001] zone axis. GeSn (111) planes overlap with β-Sn (200) [depicted with red circles in Fig. 2(b)], which is consistent with reported results.[25,26] The changes in the GeSn layer, mainly material transport by diffusion, can be seen at this stage also in the EDXS element map in Fig. 2(c). It is important to note that with the temperature increase, at 500 °C, Ga diffused from the W capping layer deposited in FIB, where it is located at room temperature, to the interface of sputtered W layer and GeSn epilayer. At 550 °C, W is diffused to the GeSn layer due to the presence of Ga.

Comparing this result with the literature data,[27–30] our sample has higher thermal stability. The beginning of Sn segregation for 50 nm thick GeSn layers with 10 at.% Sn grown by MBE has been reported to be above 230[27] and 420 °C.[28] The main difference between these two works is that the samples were annealed under quasi-equilibrium conditions[27] and used rapid thermal annealing (RTA).[28] The latter shortens the time of high-temperature exposure to the sample, minimizing the possible Sn diffusion. In particular, it has been reported that the formation of liquid-Sn segregated on the free surface of the specimen induces an efficient phase separation at lower temperatures,[27] and the absence of a liquid phase increases the thermal stability of GeSn.[31] Since the formation of the liquid phase starts at dislocations or other defects, reducing defect density through microstructuring the layers can improve the thermal stability of GeSn films.[32] We also believe that the restriction of the area, from which segregated Sn can be collected, additionally mitigates liquid drop formation at elevated temperatures. Common for both investigations[27,28] is that Sn segregation occurs before strain relaxation regardless of the heating rate. For significantly thicker GeSn samples, the strain relaxation process has been observed before the Sn segregation.[28,29] The reported Sn segregation in these GeSn layers with 10 at.% Sn occurs at 400 °C (450 nm thick, quasi-equilibrium annealing),[29] 470 °C (250 nm thick, RTA),[28] and 500 °C (120 nm thick).[30] It is clear that a relation exists between the annealing conditions and the Sn segregation temperature. All the experiments reported were performed for GeSn layers on bulk materials. In our investigation, the lamella has a thickness of only ≈100 nm, i.e., the thin foil has a large surface–volume ratio, which can introduce distinct annealing behaviors. Additionally, during the FIB thinning, the sample partially relaxed and the Sn segregation appeared in relaxed GeSn layers at higher temperatures.[33]

The STEM image of sample B taken at room temperature is represented in Fig. 3(a). The sample contains dislocations in the atypical thin Ge buffer spreading from the Si substrate interface to the GeSn layer, indicating the full or partial relaxation of this thin Ge buffer. Following the heating experiment protocol used for sample A, sample B was annealed from 25 to 300 °C. At 200 °C, the specimen of sample B rapidly decomposes under the influence of the present FIB-induced Ga contamination (supplementary material video). EDXS maps taken at room temperature after being heated at 300 °C [Fig. 3(b)] show that all Ge from the thin electron-transparent lamella region of GeSn and the Ge buffer layer is located out of the original area. This diffusion eventually leads to the formation of a GaSn alloy on the right side, a Ge-rich SiGe alloy on the left side, and a Sn-rich layer at the top of these two alloys. The phase diagram of GaGe[34] and GaSn[35] suggests that due to the much lower eutectic temperature for GaSn, a GaSn melt is formed first during heating. Then, the increased diffusion rate in the occurring liquid phase governs the ongoing decomposition process. The melt consumes the Ga-contaminated crystalline Ge buffer and GeSn layer, leading to further Ga accumulation through Ga diffusion from thicker regions of the lamella. In Fig. 3(b), it is evident that the flat interface and overall layered structure of the specimen were lost during heating, giving place to a concave form of the GaSn region. This is caused by the formation of the liquid phase at high temperatures, whose shape is preserved after cooling. Ge, containing some traces of Si, solidifies at the existing crystalline Ge regions on the left side of the GaSn melt. Similar processes were monitored during the decomposition of GeSn layers with a free, uncapped GeSn surface and are expected as the decomposition mechanism during *in situ*

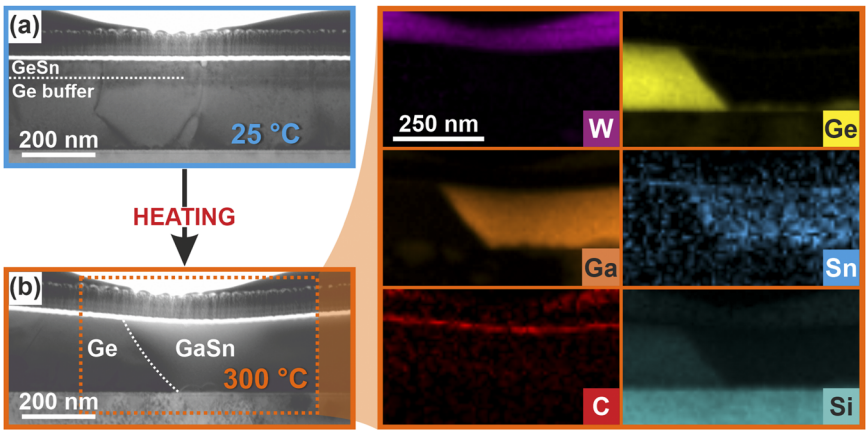

FIG. 3. (a) BF STEM image of sample B at room temperature and (b) BF STEM image after heating the specimen to 300 °C with EDXS elemental maps. At 300 °C, a GaSn alloy is formed where the Ge buffer and GeSn layer were previously located, Ge crystals are formed in the vicinity of GaSn, and a Sn top-most layer appears.

experiments as soon as liquid Sn droplets are formed.[27] Additionally, the presence of Ga strongly influences the melt properties of Sn and hence the observed critical temperatures.

The room temperature EDXS maps (see Fig. 1) show that sample B is more susceptible to Ga ion incorporation than sample A. This could indicate a higher defect density in this GeSn layer caused by the atypically thin Ge buffer layer, as it was mentioned before. Consequently, we believe that the combination of a high point defect density and local heating by the ion beam increases the diffusion rate of Ga[36] into the crystalline matrix. Assali *et al.*[37] studied GeSn CVD samples via positron annihilation spectroscopy and found that the dominant point defect is a divacancy independent of the Sn content. Here, it is essential to emphasize that the FIB sample preparation for both samples followed the same protocols. Since sample A did not exhibit the same susceptibility for Ga contamination, it is safe to assume that sample B differs from sample A in one structural property, for which a higher point defect density is a probable candidate. Considering that sample B was grown at a higher temperature, it was expected to have fewer point defects than sample A. The presence of H_2 in the precursors of the CVD growth process and the higher growth rates could lead, on the other hand, to more point defects compared to the MBE-grown sample. However, ultimately, the results probably show the important role of a high-quality substrate: the use of the atypical thin Ge buffer with low quality has led to a sample with a high density of point defects. Thus, our results emphasize the crucial role of using a thick Ge virtual substrate and the indispensable need to keep point defect density low to improve thermal stability and suppress detrimental Sn segregation.

IV. CONCLUSIONS

In summary, we found, on the one hand, that the GeSn layer of a sample grown on a commercial Ge substrate (sample A) exhibits a low defect density and is stable up to 500 °C in our *in situ* TEM experiment. On the other hand, if a GeSn layer is grown on a lesser substrate—even CVD growth is employed (sample B)—it leads to a higher point defect density. Due to defects, the sample is highly susceptible to Ga incorporation and exhibits a much lower decomposition temperature. For the thermal behavior of these samples, we argue that, generally, two different mechanisms of efficient phase separation are present: solid-state diffusion and liquid-phase formation. For sample A, a solid-state diffusion and precipitation mechanism occurs since the formation of a liquid phase seems to be suppressed. Due to the even distribution of the atoms because of the used slow growth rates and the coverage of the free surface with a W capping layer, fast diffusion of the Sn over surfaces or defects was inhibited, and the decomposition started at relatively high temperatures as solid-state precipitation. The coverage of the free surface is vital because, in similar samples from earlier studies, liquid phase formation of the Sn phase was observed at significantly lower temperatures.[27] Our results indicate that one needs measures to avoid liquid phase formation for fabricating stable GeSn compounds with Sn contents higher than 10 at.%, which is in line with the findings reported in Ref. 31. If an efficient Sn segregation cannot be suppressed, e.g., due to inherent defects in the material, liquid phase formation determines the stability of the alloy. This is relevant for our investigated sample B, which exhibits an intentionally higher defect density, caused by the atypically thin Ge buffer layer. First, this was assessed via an enhanced susceptibility of this sample to the Ga incorporation of the FIB preparation process. After the *in situ* MEMS chip loading, we observed an unexpectedly high Ga contamination in our lamella. Second, we monitored a liquid phase formation at ≈200 °C. Hereby, the liquid phase formation was additionally triggered by the presence of Ga contamination introduced by FIB preparation. Even if the determined temperatures are not reliable due to the eutectic formation by Ga, we can clearly see a different decomposition mode present in the *in situ* TEM experiment of sample B. Taking into account the behavior of this sample under Ga-illumination, the incorporation of Ga into the defect structure of a crystal during a FIB process could be used as a qualitative method to compare the defect density of different samples, i.e., Ga can act as a contrast agent for point defects. The point defect density not only disturbs the optical properties but also seems to have a dramatic influence on the decomposition mode. Further experiments applying Ga-free or reduced preparation methods are on the way to refine our gained results.

SUPPLEMENTARY MATERIAL

The supplementary material video is provided online, where the decomposition of the sample B under the influence of the present FIB-induced Ga contamination can be observed.

ACKNOWLEDGMENTS

We would like to thank Karin Stadlmann for the preparation of conventional cross-sectional/wedge-polished TEM samples. We acknowledge the financial support from the Austrian Federal Ministry of Labor and Economy; the National Foundation for Research, Technology, and Development; and the Christian Doppler Research Association. We also acknowledge support from the Austrian Science Fund, FWF, via Project No. Y1238-N36.

AUTHOR DECLARATIONS

Conflict of Interest

The authors have no conflicts to disclose.

Author Contributions

Karí Martínez: Data curation (equal); Investigation (equal); Methodology (equal); Validation (equal); Visualization (equal); Writing – original draft (equal); Writing – review & editing (equal). **Alexey Minenkov**: Conceptualization (equal); Investigation (equal); Methodology (equal); Supervision (equal); Validation (equal); Writing – original draft (equal); Writing – review & editing (equal). **Johannes Aberl**: Methodology (equal); Writing – review & editing (equal). **Dan Buca**: Resources (equal); Writing – review & editing (equal). **Moritz Brehm**: Funding acquisition (supporting); Methodology (equal); Resources (equal); Writing – review & editing (equal). **Heiko Groiss**: Conceptualization (equal); Funding acquisition (lead); Methodology (equal); Project administration

(lead); Resources (equal); Supervision (equal); Validation (equal); Writing – original draft (equal); Writing – review & editing (equal).

DATA AVAILABILITY

The data that support the findings of this study are available from the corresponding author upon reasonable request.

REFERENCES

[1] S. Gupta, B. Magyari-Köpe, Y. Nishi, and K. C. Saraswat, "Achieving direct band gap in germanium through integration of Sn alloying and external strain," J. Appl. Phys. **113**(7), 73707 (2013).

[2] R. Chen, H. Lin, Y. Huo, C. Hitzman, T. I. Kamins, and J. S. Harris, "Increased photoluminescence of strain-reduced, high-Sn composition $Ge_{1-x}Sn_x$ alloys grown by molecular beam epitaxy," Appl. Phys. Lett. **99**(18), 181125 (2011).

[3] J. Zheng *et al.*, "Recent progress in GeSn growth and GeSn-based photonic devices," J. Semicond. **39**(6), 061006 (2018).

[4] J. Doherty *et al.*, "Progress on germanium–tin nanoscale alloys," Chem. Mater. **32**(11), 4383–4408 (2020).

[5] A. Minenkov and H. Groiss, "Evolution of phases and their thermal stability in Ge–Sn nanofilms: A comprehensive *in situ* TEM investigation," J. Alloys Compd. **859**, 157763 (2021).

[6] R. Cheng *et al.*, "Mobility enhancement techniques for Ge and GeSn MOSFETs," J. Semicond. **42**(2), 023101 (2021).

[7] C.-P. Chou, Y.-X. Lin, Y.-K. Huang, C.-Y. Chan, and Y.-H. Wu, "Junctionless poly-GeSn ferroelectric thin-film transistors with improved reliability by interface engineering for neuromorphic computing," ACS Appl. Mater. Interfaces **12**(1), 1014–1023 (2019).

[8] A. Minenkov *et al.*, "Advanced preparation of plan-view specimens on a MEMS chip for *in situ* TEM heating experiments," MRS Bull. **47**(4), 359–370 (2022).

[9] X. Zhong *et al.*, "Comparing Xe^+pFIB and Ga^+FIB for TEM sample preparation of Al alloys: Minimising FIB-induced artefacts," J. Microsc. **282**(2), 101–112 (2021).

[10] Y. J. Xiao, F. Z. Fang, Z. W. Xu, W. Wu, and X. C. Shen, "The study of Ga^+ FIB implanting crystal silicon and subsequent annealing," Nucl. Instrum. Methods Phys. Res., Sect. B **307**, 253–256 (2013).

[11] M. Oehme, K. Kostecki, M. Schmid, F. Oliveira, E. Kasper, and J. Schulze, "Epitaxial growth of strained and unstrained GeSn alloys up to 25% Sn," Thin Solid Films **557**, 169–172 (2014).

[12] S. Wirths *et al.*, "Lasing in direct-bandgap GeSn alloy grown on Si," Nat. Photonics **9**(2), 88–92 (2015).

[13] L. Zhang *et al.*, "Structural property study for GeSn thin films," Materials **13**(16), 3645 (2020).

[14] D. Buca *et al.*, "Room temperature lasing in GeSn microdisks enabled by strain engineering," Adv. Opt. Mater. **10**(22), 2201024 (2022).

[15] J. Margetis *et al.*, "Si-based GeSn lasers with wavelength coverage of 2–3 μm and operating temperatures up to 180 K," ACS Photonics **5**(3), 827–833 (2017).

[16] Q. M. Thai *et al.*, "GeSn heterostructure micro-disk laser operating at 230 K," Opt. Express **26**(25), 32500–32508 (2018).

[17] O. Nakatsuka *et al.*, "(Invited) heteroepitaxial growth of Sn-related group-IV materials on Si platform for microelectronic and optoelectronic applications: Challenges and opportunities," ECS Trans. **58**(9), 149 (2013).

[18] J. Nicolas, S. Assali, S. Mukherjee, A. Lotnyk, and O. Moutanabbir, "Dislocation pipe diffusion and solute segregation during the growth of metastable GeSn," Cryst. Growth Des. **20**(5), 3493–3498 (2020).

[19] J. M. Hartmann, A. Abbadie, N. Cherkashin, H. Grampeix, and L. Clavelier, "Epitaxial growth of Ge thick layers on nominal and 6° off Si(0 0 1); Ge surface passivation by Si," Semicond. Sci. Technol. **24**(5), 055002 (2009).

[20] A. Salomon, J. Aberl, L. Vukušić, M. Hauser, T. Fromherz, and M. Brehm, "Relaxation delay of Ge-rich epitaxial SiGe films on Si(001)," Phys. Status Solidi A **219**(17), 2200154 (2022).

[21] L. Wind *et al.*, "Composition dependent electrical transport in $Si_{1-x}Ge_x$ nanosheets with monolithic single-elementary Al contacts," Small **18**(44), 2204178 (2022).

[22] J. Tijn van Omme, M. Zakhozheva, R. G. Spruit, M. Sholkina, and H. H. Pérez Garza, "Advanced microheater for *in situ* transmission electron microscopy; enabling unexplored analytical studies and extreme spatial stability," Ultramicroscopy **192**, 14–20 (2018).

[23] E. I. Preiß *et al.*, "Applicability of focused Ion beam (FIB) milling with gallium, neon, and xenon to the fracture toughness characterization of gold thin films," J. Mater. Res. **36**, 2505–2514 (2021).

[24] T. C. Pekin, F. I. Allen, and A. M. Minor, "Evaluation of neon focused ion beam milling for TEM sample preparation," J. Microsc. **264**(1), 59–63 (2016).

[25] S. Takeuchi, A. Sakai, O. Nakatsuka, M. Ogawa, and S. Zaima, "Tensile strained Ge layers on strain-relaxed $Ge_{1-x}Sn_x$/virtual Ge substrates," Thin Solid Films **517**(1), 159–162 (2008).

[26] S. Liu *et al.*, "Growth of α-Sn on silicon by a reversed β-Sn to α-Sn phase transformation for quantum material integration," Commun. Mater. **3**(1), 17 (2022).

[27] H. Groiss *et al.*, "Free-running Sn precipitates: An efficient phase separation mechanism for metastable $Ge_{1-x}Sn_x$ epilayers," Sci. Rep. **7**(1), 16114 (2017).

[28] H. Cai *et al.*, "Thickness-dependent behavior of strain relaxation and Sn segregation of GeSn epilayer during rapid thermal annealing," J. Alloys Compd. **904**, 164068 (2022).

[29] L. Wang *et al.*, "Effects of annealing on the behavior of Sn in GeSn alloy and GeSn-based photodetectors," IEEE Trans. Electron Devices **67**(8), 3229–3234 (2020).

[30] J. Spièce *et al.*, "Quantifying thermal transport in buried semiconductor nanostructures via cross-sectional scanning thermal microscopy," Nanoscale **13**(24), 10829–10836 (2021).

[31] M. S. Seifner, S. Hernandez, J. Bernardi, A. Romano-Rodriguez, and S. Barth, "Pushing the composition limit of anisotropic $Ge_{1-x}Sn_x$ nanostructures and determination of their thermal stability," Chem. Mater. **29**(22), 9802–9813 (2017).

[32] V. Bonino *et al.*, "Microstructuring to improve the thermal stability of GeSn layers," ACS Appl. Mater. Interfaces **14**(19), 22270–22277 (2022).

[33] P. Zaumseil *et al.*, "The thermal stability of epitaxial GeSn layers," APL Mater. **6**(7), 076108 (2018).

[34] I. Ansara, J. P. Bros, and M. Gambino, "Thermodynamic analysis of the germanium-based ternary systems (Al Ga Ge, Al Ge Sn, Ga Ge Sn)," Calphad **3**(3), 225–233 (1979).

[35] T. J. Anderson and I. Ansara, "The Ga-Sn (gallium-tin) system," J. Phase Equilib. **13**, 181–189 (1992).

[36] D. J. Barber, "Radiation damage in ion-milled specimens: Characteristics, effects and methods of damage limitation," Ultramicroscopy **52**(1), 101–125 (1993).

[37] S. Assali *et al.*, "Vacancy complexes in nonequilibrium germanium-tin semiconductors," Appl. Phys. Lett. **114**(25), 251907 (2019).